Computers and Mathematics with Applications 63 (2012) 1433–1441

Contents lists available at SciVerse ScienceDirect

Computers and Mathematics with Applications

journal homepage: www.elsevier.com/locate/camwa

3D vector tomography using vector spherical harmonics decomposition

A.L. Balandin [a,*], Y. Ono [b], S. You [c]

[a] Institute of Systems Dynamics and Control Theory, Lermontov Str. 134, 664033, Irkutsk-33, Russia
[b] High Temperature Plasma Center, University of Tokyo, 2–11–16 Yayoi, Bunkyo–ku, Tokyo 113–8656, Japan
[c] University of Washington, Seattle, WA, USA

ARTICLE INFO

Article history:
Received 25 March 2011
Received in revised form 23 December 2011
Accepted 15 March 2012

Keywords:
Numerical methods
Inverse problems
Computerized tomography
Spherical harmonics

ABSTRACT

The article presents the reconstruction method of the flow fields from vector tomography passive ion Doppler spectroscopy in a plasma experiment. The method is based on series expansion in terms of vector spherical harmonics for volumetric, divergent-free vector fields and intended for three-dimensional diagnostic in the spherical tokamak devices. An inversion of spectral experimental data is known in tomography as an inversion of vectorial ray transform. The relation of the vectorial ray transform with Doppler spectroscopy measurements are given in Balandin and Ono (2001, 2003) [7,8]. The effectiveness of the proposed method is tested on a range of model 3D divergent-free vector fields.

1. Introduction

Tomographic reconstruction of scalar fields in plasmas from passive spectroscopic measurements is a well established technique for non-invasive measurements of internal plasma structure [1,2]. Scalar tomography techniques have, for example, resolved plasma shapes in tokamaks during sawtooth crashes from X-ray emission [3] and imaged the kink instability in a magnetoplasmadynamic thruster from ultraviolet line emission [4]. Tomographic reconstruction of vector fields in plasmas, however, has only been proposed more recently [5–9]. Vector Spherical Harmonics (VSHs) (as well as tensor spherical harmonics) occur in many fields of engineering and theoretical physics. In particular, they are used in quantum mechanics [10–12], or whenever one has to deal with vector fields of any geophysical nature [13,14]. Freeden in [15] give an application of VSHs to geoscientific problems. While VSHs have been long used in electromagnetic theory [16] and quantum mechanics [17], it is only recently that they have been applied in vector tomography problems. Various applications have led to different ways of definition of vector and tensor spherical harmonics, putting the accent on issues [11,12,16,18]. The comparison of VSHs defined by different authors are given in [18, p. 234].

This paper is an attempt to extend the use of VSHs to real computations in vector tomography diagnostics of spherical tokamak plasmas. The basic formulas used for spherical vector theory are reviewed in [18].

The vector field is considered in the laboratory coordinate system $S = (\mathbf{e}_1, \mathbf{e}_2, \mathbf{e}_3)$, with Euclidean coordinates $\mathbf{x} = (x, y, z)$ and may be subjected to any rotation $\mathcal{R}$ ($\mathcal{R}$ is an element of the rotation group SO(3)). This rotation transforms the vector field $\mathbf{g}(\mathbf{x})$ to a new vector field $\mathbf{g}'(\mathbf{x}')$. Thus, each rotation of the group SO(3) is in correspondence with a linear transformation $T_{\mathcal{R}}$ acting in the following manner:

$$\mathbf{g}'(\mathbf{x}') = T_{\mathcal{R}}\mathbf{g}(\mathbf{x}) = \mathcal{R}\mathbf{g}(\mathcal{R}^{-1}\mathbf{x}). \tag{1}$$

* Corresponding author.
E-mail address: balandin@icc.ru (A.L. Balandin).

0898-1221/$ – see front matter © 2012 Elsevier Ltd. All rights reserved.
doi:10.1016/j.camwa.2012.03.049

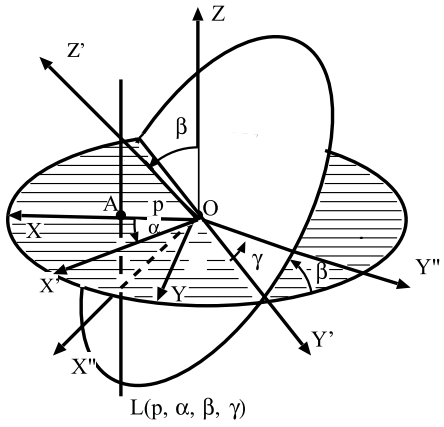

Fig. 1. Integration path $L(p, \alpha, \beta, \gamma)$ and Euler angles for the ray transformation; xyz and $x'y'z'$ are, respectively, the laboratory coordinate system and the coordinate systems for a vector field. Integration is performed along the z axis with different values of the angles α, β, and γ, with $p = OA$.

Expanding vector fields requires basis functions to be chosen so that any operation of the transformation group SO(3) yields a linear combination of the basis functions. For instance, radial vector fields in a spherical coordinate system are transformed by rotation in exactly the same way as are scalar fields; consequently, as the basis for the subspace of entirely radial vector fields we can take vector functions $Y_{JM}(\theta, \varphi)\mathbf{e}_r$, where $\mathbf{e}_r$ are unit radial vectors in the spherical coordinate system and $Y_{JM}(\theta, \varphi)$ are scalar spherical harmonics [19]. Thus, radial vector fields can be studied with the use of scalar spherical harmonics.

For an arbitrary vector field, each component of the vector function $\mathbf{g}(\mathbf{x})$ can also be expanded into a series with respect to scalar spherical harmonics, but the field components become mixed owing to rotation, and the coefficient matrix will be of full rank and of considerable size [9]. Representation of the vector field via VSHs is justified by the following properties of these harmonics (see Appendix B):

$$\nabla \cdot [f(r)\mathbf{Y}^{(0)}_{JM}(\theta, \varphi)] = 0, \qquad \nabla \cdot [f(r)\mathbf{Y}^{(\pm 1)}_{JM}(\theta, \varphi)] \neq 0$$

for all functions $f(r) \neq 0$ and $\mathbf{Y}^{(\lambda)}_{JM}(\theta, \varphi)$ are vector spherical harmonics. Thus, VSHs naturally divide the vector field into the solenoidal and potential components; correspondingly, we can form bases for the solenoidal and potentional vector fields.

As the spectral Doppler data allow only the solenoidal component of the field to be reconstructed, below we assume that $\nabla \cdot \mathbf{g}(\mathbf{x}) = 0$. The measurements are supposed to be performed in a laboratory coordinate system S along the z axis. Rotation is considered as an active process, i.e., as rotation of the vector field in a fixed coordinate system S, [20]. The rotation matrix $\mathcal{R}(\alpha, \beta, \gamma)$ maps the vector $\mathbf{x}$ in the laboratory coordinate system S to a new vector $\mathbf{x}'$ in a vector field coordinate system S', and we write $\mathbf{x} = \mathcal{R}(\alpha, \beta, \gamma)\mathbf{x}'$, where Euler angles (α, β, γ) are determined in the same way as in [18]. Now β and α are the polar and azimuthal angles of the axis z' in the coordinate system S (see Fig. 1). For an arbitrary rotation determined by positive Euler angles (α, β, γ), the rotation matrix is written in the form[1]

$$\mathcal{R} = \left(\begin{array}{c|c|c} \cos\alpha\cos\beta\cos\gamma - \sin\alpha\sin\gamma & -\cos\alpha\cos\beta\sin\gamma - \sin\alpha\cos\gamma & \cos\alpha\sin\beta \\ \sin\alpha\cos\beta\cos\gamma + \cos\alpha\sin\gamma & -\sin\alpha\cos\beta\sin\gamma + \cos\alpha\cos\gamma & \sin\alpha\sin\beta \\ -\sin\beta\cos\gamma & \sin\beta\sin\gamma & \cos\beta \end{array}\right),$$

$$0 \leq \alpha < 2\pi, \qquad 0 \leq \beta \leq \pi, \qquad 0 \leq \gamma < 2\pi.$$

The paper is organized as follows. The representation of the solenoidal vector field is given in Section 2. An inversion method is described in Section 3. Results of numerical simulation are given in Section 4. Appendix A provides the definition of Wigner D-functions and the method for calculating these. The definition of vector spherical harmonics and some of their properties are given in Appendix B.

2. Representation of the solenoidal vector field

In the space $\mathbb{R}^3$, a unit ball and unit sphere are defined to be $\mathbb{B}^3 = \{\mathbf{x} \in \mathbb{R}^3 \mid |\mathbf{x}| < 1\}$ and $\mathbb{S}^2 := \{\boldsymbol{\omega} \in \mathbb{R}^3 \mid |\boldsymbol{\omega}| = 1\} = \partial\mathbb{B}^3$. We assume that the vector field $\mathbf{g}(\mathbf{x})$ is reconstructed in the unit ball has zero values of the normal component on the boundary, and belongs to the Sobolev space [21], i.e.,

$$H_0(\mathrm{div}; \mathbb{B}^3) := \{\mathbf{g} \in \mathbf{L}_2(\mathbb{B}^3) \mid \mathrm{div}\,\mathbf{g} = 0,\ \boldsymbol{\nu} \cdot \mathbf{g}(\mathbf{x}) = 0,\ \mathbf{x} \in \partial\mathbb{B}^3\}.$$

[1] The angle is positive if the rotation appears to be counterclockwise with respect to an observer looking towards the origin.

It is known that the Helmholtz–Hodge expansion, in this instance, lacks in a harmonic vector component [22]. As the set $\mathbf{Y}^{(\lambda)}_{JM}$ forms an orthogonal basis in $\mathbf{L}_2(\mathbb{S}^2)$ (see Appendix B), an arbitrary vector field $\mathbf{g}(\mathbf{x})$ satisfying the condition

$$\int |\mathbf{g}(r\boldsymbol{\omega})|^2 d\boldsymbol{\omega} < \infty \quad \text{with} \int d\boldsymbol{\omega} \equiv \int_0^{\pi} d\theta \sin\theta \int_0^{2\pi} d\varphi, \quad 0 < r \le 1,$$

can be represented, in its own coordinate system, as a series

$$\mathbf{g}(\mathbf{x}') = \sum_{\lambda} \sum_{\substack{J=0,\\ |M_2|\le J}}^{\infty} \mathrm{g}^{(\lambda)}_{JM_2}(r)\mathbf{Y}^{(\lambda)}_{JM_2}(\boldsymbol{\omega}'), \quad \mathbf{x}' = r\boldsymbol{\omega}',\ \boldsymbol{\omega}' = (\theta', \varphi'),\ \lambda = -1, 0, 1. \tag{2}$$

or, in invariant form

$$\mathbf{g}(\mathbf{x}) = \sum_{\lambda} \sum_{\substack{J=0,\\ |M_2|\le J,\\ |M_1|\le J}}^{\infty} \mathrm{g}^{(\lambda)}_{JM_2}(r)\, D^{J}_{M_1M_2}(\alpha, \beta, \gamma)\mathbf{Y}^{(\lambda)}_{JM_1}(\boldsymbol{\omega}'), \quad \mathbf{x} = r\boldsymbol{\omega},\ \boldsymbol{\omega} = (\theta, \varphi), \tag{3}$$

where $D^{J}_{M_1M_2}(\alpha, \beta, \gamma)$ are Wigner D-functions and $\mathbf{Y}^{(\lambda)}_{JM_1}(\boldsymbol{\omega})$ are vector spherical harmonics.

To satisfy the condition of being solenoidal for a field, we use Eq. (34) of Appendix B and impose the following constraints on the functions $\mathrm{g}^{(-1)}_{JM_2}(r)$ and $\mathrm{g}^{(+1)}_{JM_2}(r)$ in Eq. (3):

$$\mathrm{g}^{(-1)}_{JM_2}(r) = i\sqrt{J(J+1)}\frac{1}{r}\mathrm{g}^{(00)}_{JM_2}(r), \qquad \mathrm{g}^{(+1)}_{JM_2}(r) = i\left(\frac{d}{dr} + \frac{1}{r}\right)\mathrm{g}^{(00)}_{JM_2}(r), \tag{4}$$

where $\mathrm{g}^{(00)}_{JM_2}(r)$ is an arbitrary differentiable function. In this case Eq. (3) is rewritten thus:

$$\mathbf{g}(\mathbf{x}) = \sum_{\substack{J=0,\\ |M_1|\le J,\\ |M_2|\le J}}^{\infty} D^{J}_{M_1M_2}(\alpha, \beta, \gamma)\{\mathrm{g}^{(0)}_{JM_2}(r)\mathbf{Y}^{(0)}_{JM_2}(\boldsymbol{\omega}') + \nabla \times [\mathrm{g}^{(00)}_{JM_2}(r)\mathbf{Y}^{(0)}_{JM_2}(\boldsymbol{\omega}')]\}, \tag{5}$$

and the solenoidal condition $\nabla \cdot \mathbf{g}(\mathbf{x}) = 0$ is satisfied. Thus, Eq. (5) is an expansion of an arbitrary solenoidal vector field in terms of VSHs $\mathbf{Y}^{(\lambda)}_{JM_2}(\boldsymbol{\omega})$. Since each solenoidal field under rotation remains solenoidal, the field components do not become mixed in such a representation [23].

3. Inversion procedure

The task of 3D vector tomography is to reconstruct a vector field $\mathbf{g}(\mathbf{x})$in a space $\mathbb{B}^3$ from a certain set of projection data, i.e., from its ray transformation. In the general form, projection data can be written

$$(\mathcal{X}\mathbf{g})(\mathbf{x}, \mathbf{n}) \equiv \check{\mathrm{g}}(\mathbf{x}, \mathbf{n}) = \int_{-\infty}^{\infty} \mathbf{g}(\mathbf{x} + l\mathbf{n}) \cdot \boldsymbol{\chi}(\mathbf{n}) dl, \tag{6}$$

where $\mathbf{n}$ is a unit vector aligned along the observation line; the vector function $\boldsymbol{\chi}$ depends on the physical method of measurement; for spectral measurements, we have $\boldsymbol{\chi}(\mathbf{n}) \equiv \mathbf{n}$.

It is known, that there are two classes of tomographic projections of vector fields. The first type includes integration of a field component directed along the observation line (spectral measurements). The second type involves integration of a field transverse component (NMR measurements). In the first case the central section theorem applies, and only the solenoidal component of a field can be reconstructed from projection data. Measurements of the second type allow a potential component of the field to be calculated [24].

Rotation of the coordinate system S' with respect to the coordinate system S is chosen so that the integration line representing the projection data is directed along the z axis, and the angle φ can be set to zero in the laboratory coordinate system. In this case the projection data (6) are written in the form

$$\check{\mathrm{g}}(p, \alpha, \beta, \gamma) = \int_{-\infty}^{\infty} dz \sum_{\lambda=-1,0,+1} \sum_{J, M_2, M_1} \mathrm{g}^{(\lambda)}_{JM_2}(r)\, D^{J}_{M_1M_2}(\alpha, \beta, \gamma)\, \mathbf{e}_z \cdot \mathbf{Y}^{(\lambda)}_{JM_1}(\boldsymbol{\omega}'). \tag{7}$$

It seems convenient to present Eq. (7) by the following two relations:

$$\check{\mathrm{g}}(p, \alpha, \beta, \gamma) = \sum_{J, M_2, M_1} D^{J}_{M_1M_2}(\alpha, \beta, \gamma)\, G^{J}_{M_1M_2}(p), \tag{8}$$

$$G^{J}_{M_1M_2}(p) = \sum_{\lambda} \int_{-\infty}^{\infty} dz\, \mathrm{g}^{(\lambda)}_{JM_2}(r)\, \mathbf{e}_z \cdot \mathbf{Y}^{(\lambda)}_{JM_1}(\boldsymbol{\omega}'). \tag{9}$$

The functions $G^J_{M_1M_2}(p)$ can be found from the experimental data $\check{\mathrm{g}}(p,\alpha,\beta,\gamma)$, based on the orthogonality property for Wigner D-functions under the condition that a large number of measurements are available. We obtain

$$G^J_{M_1M_2}(p) = \frac{2J+1}{8\pi^2}\int_0^{2\pi} d\alpha \int_0^{\pi} \sin\beta d\beta \int_0^{2\pi} d\gamma\, \check{\mathrm{g}}(p,\alpha,\beta,\gamma)\, D^{J*}_{M_1M_2}(\alpha,\beta,\gamma), \tag{10}$$

where the asterisk means complex conjugation.

In the opposite case, we can use the least squares technique [25]. Thus, below we assume that the functions $G^J_{M_1M_2}(p)$ are known and can be used to calculate the unknown functions $\mathrm{g}^{(\lambda)}_{JM_2}(r)$ in (9). There is no loss of generality in computing the scalar product in (9) for $\varphi = 0$. As a result, we obtain

$$\mathbf{Y}^{(-1)}_{JM}(\theta,\varphi=0)\cdot\mathbf{e}_z = N_{JM}\,\cos(\theta)P^M_J(\cos(\theta)), \tag{11}$$

$$\mathbf{Y}^{(0)}_{JM}(\theta,\varphi=0)\cdot\mathbf{e}_z = \frac{N_{JM}\,M}{\sqrt{J(J+1)}}P^M_J(\cos(\theta)), \tag{12}$$

$$\mathbf{Y}^{(1)}_{JM}(\theta,\varphi=0)\cdot\mathbf{e}_z = \frac{N_{JM}}{\sqrt{J(J+1)}}\big[(J+1)\,\cos(\theta)\,P^M_J(\cos(\theta)) - (J-M+1)\,P^M_{J+1}(\cos(\theta))\big], \tag{13}$$

where $\cos(\theta) = \sqrt{1-p^2/r^2}$, $N_{JM} = 1/\|Y_{JM}\|_{L_2}$ and $P^M_J(x)$ are adjoined Legendre polynomials.

Our present goal is to calculate the right-hand side of Eq. (9) with allowance for constraints (4). We have

$$\int_{-\sqrt{1-p^2}}^{\sqrt{1-p^2}} dz\, \mathrm{g}^{(0)}_{JM_2}(r)\,\mathbf{e}_z\cdot\mathbf{Y}^{(0)}_{JM_1}(\theta,\varphi=0) = C_1\int_p^1 \frac{P^{M_1}_J\left(\sqrt{1-p^2/r^2}\right)\mathrm{g}^{(0)}_{JM_2}(r)\,dr}{\sqrt{1-p^2/r^2}} \tag{14}$$

$$\int_{-\sqrt{1-p^2}}^{\sqrt{1-p^2}} dz\,\left(i\sqrt{J(J+1)}/r\right)\mathrm{g}^{(00)}_{JM_2}(r)\,\mathbf{e}_z\cdot\mathbf{Y}^{(-1)}_{JM_1}(\theta,\varphi=0) = i\,C_2\int_p^1 \frac{P^{M_1}_J\left(\sqrt{1-p^2/r^2}\right)\mathrm{g}^{(00)}_{JM_2}(r)\,dr}{r} \tag{14'}$$

$$\begin{aligned}\int_{-\sqrt{1-p^2}}^{\sqrt{1-p^2}} dz\, i(d/dr+1/r)\,\mathrm{g}^{(00)}_{JM_2}(r)\,\mathbf{e}_z\cdot\mathbf{Y}^{(+1)}_{JM_1}(\theta,\varphi=0) &= i\,C_3\int_p^1 P^{M_1}_J\left(\sqrt{1-p^2/r^2}\right)(d/dr+1/r)\,\mathrm{g}^{(00)}_{JM_2}(r)\,dr\\ &\quad - i\,C_4\int_p^1 \frac{P^{M_1}_{J+1}\left(\sqrt{1-p^2/r^2}\right)(d/dr+1/r)\,\mathrm{g}^{(00)}_{JM_2}(r)\,dr}{\sqrt{1-p^2/r^2}}\end{aligned} \tag{14''}$$

$$\begin{aligned}C_1 &= \frac{M_1N_{JM_1}(1+(-1)^{J+M_1})}{\sqrt{J(J+1)}}, \qquad C_2 = N_{JM_1}\sqrt{J(J+1)}\,(1+(-1)^{J+M_1}),\\ C_3 &= \frac{N_{JM_1}(J+1)(1+(-1)^{J+M_1})}{\sqrt{J(J+1)}}, \qquad C_4 = \frac{N_{JM_1}(J-M_1+1)(1-(-1)^{J+M_1})}{\sqrt{J(J+1)}}.\end{aligned} \tag{15}$$

From Eqs. (14) we can see that the functions $\mathrm{g}^{(0)}_{JM_2}$ satisfy the following Volterra equation:

$$\begin{aligned}Re\{G^J_{M_1M_2}(p)\} &= \int_p^1 \mathcal{K}_1(p,r)\mathrm{g}^{(0)}_{JM_2}(r)\,dr\\ &\equiv \frac{(1+(-1)^{J+M_1})M_1N_{JM_1}}{\sqrt{J(J+1)}}\int_p^1 \frac{P^{M_1}_J\left(\sqrt{1-p^2/r^2}\right)\mathrm{g}^{(0)}_{JM_2}(r)\,dr}{\sqrt{1-p^2/r^2}},\end{aligned} \tag{16}$$

The functions $\mathrm{g}^{(00)}_{JM_2}$ meet, respectively, (17), (18) with even and odd values of $J+M_1$, i.e.,

$$\begin{aligned}Im\{G^J_{M_1M_2}(p)\} &= \int_p^1 \mathcal{K}_2(p,r)f^{(+)}_{JM_2}(r)\,dr\\ &\equiv (1+(-1)^{J+M_1})N_{JM_1}\sqrt{\frac{J+1}{J}}\int_p^1 P^{M_1}_J\left(\sqrt{1-p^2/r^2}\right)\left(\frac{d}{dr}+\frac{J+1}{r}\right)\mathrm{g}^{(00)}_{JM_2}(r)\,dr.\end{aligned} \tag{17}$$

$$\begin{aligned}Im\{G^J_{M_1M_2}(p)\} &= \int_p^1 \mathcal{K}_3(p,r)f^{(-)}_{JM_2}(r)\,dr\\ &\equiv \frac{(1-(-1)^{J+M_1})N_{JM_1}(J-M_1+1)}{\sqrt{J(J+1)}}\int_p^1 \frac{P^{M_1}_{J+1}\left(\sqrt{1-p^2/r^2}\right)\left(\frac{d}{dr}+\frac{1}{r}\right)\mathrm{g}^{(00)}_{JM_2}(r)\,dr}{\sqrt{1-p^2/r^2}}.\end{aligned} \tag{18}$$

The function $Re\{G^J_{M_1M_2}(p)\}$ and $Im\{G^J_{M_1M_2}(p)\}$ are, respectively, the real and imaginary parts of $G^J_{M_1M_2}(p)$. Eqs. (16)–(18) can be solved by usual method of quadratures [26], since the limit of the integrand at $r = p$ is bounded.[2] Thus, the function $g^{(0)}_{JM_2}(r)$ is found from (16), and functions $f^{(\pm)}_{JM_2}(r)$ are determined from Eqs. (17) and (18) with odd and even values of $J + M_1$, respectively. The functions $g^{(-1)}_{JM_2}(r)$ and $g^{(+1)}_{JM_2}(r)$ are computed as follows

$$\begin{aligned} g^{(+1)}_{JM_2}(r) &= i f^{(-)}_{JM_2}(r) \quad \text{where } i = \sqrt{-1}, \\ g^{(-1)}_{JM_2}(r) &= i\sqrt{(J+1)/J}\left(f^{(+)}_{JM_2}(r) - f^{(-)}_{JM_2}(r)\right). \end{aligned} \tag{19}$$

The vector field is reconstructed with the use of (3). Note that there exist an analytical formula for the inversion of (16) and (18) [27], but this formula is of no practical value because of its instability.

4. Numerical simulation

To estimate the reconstruction quality in experiments, the tomographic reconstruction technique is first tested on two reference vector fields. The first model is a solenoidal vector field (for instance velocity field), which is generally described by infinitely Fourier coefficients and is written in the form

$$\begin{aligned} &\mathbf{g}(\mathbf{x}) = \nabla \times \mathbf{\Psi}(x, y, z), \quad \mathbf{\Psi} = (\psi_x, \psi_y, \psi_z), \\ &\psi_x = \exp\left(-\frac{(\rho_{yz} - \rho_x)^2}{2\sigma^2}\right), \quad \rho_{yz} = (y^2 + z^2)^{1/2}, \\ &\psi_y = \exp\left(-\frac{(\rho_{xz} - \rho_y)^2}{2\sigma^2}\right), \quad \rho_{xz} = (x^2 + z^2)^{1/2}, \\ &\psi_z = \exp\left(-\frac{(\rho_{xy} - \rho_z)^2}{2\sigma^2}\right), \quad \rho_{xy} = (x^2 + y^2)^{1/2}, \end{aligned} \tag{20}$$

$\sigma = \triangle\rho/2\sqrt{(2\ln 2)}$, $\triangle\rho = 0.7$, $\rho_x = \rho_y = \rho_z = 0.65$.

The second simulation uses a more realistic solenoidal (divergent-free) vector field with an infinite number of Fourier coefficients. The reference vector field $\mathbf{g}(\mathbf{x})$ is the Solov'ev analytical solution to the Grad–Shafranov equation [28], generally used to model magnetic plasma equilibrium. A flux function ψ and the corresponding velocity field are given by

$$\begin{aligned} &\psi(r, z) = \psi_0 \frac{r^2}{r_0^4}(2r_0^2 - r^2 - 4\zeta z^2), \\ &\mathbf{g}(r, z) = \frac{1}{2\pi r}\nabla\psi \times \mathbf{e}_\varphi, \\ &g_r(r, z) = \frac{1}{2\pi r}\frac{8\psi_0\zeta}{r_0^4} r^2 z, \\ &g_z(r, z) = \frac{1}{2\pi r}\left[-4\frac{\psi_0}{r_0^4} r^3 + 2\left(2\frac{\psi_0}{r_0^2} - 4\zeta\frac{\psi_0}{r_0^4} z^2\right) r\right], \\ &\mathbf{g}(\mathbf{x}) = (g_r(r, z)\cos(\varphi), g_r(r, z)\sin(\varphi), g_z(r, z)), \end{aligned} \tag{21}$$

where $\psi_0 = 1.0,\ r_0 = 0.7,\ \zeta = 0.2$.

The projection data (functions $\check{g}(p, \alpha, \beta, \gamma)$) were calculated on a grid $N_\alpha = N_\beta = N_\gamma = 11$ and $N_p = 10$ for the variables α, β, γ and p, respectively. The reconstructions was performed with the projection data spoiled by artificial noise with normally distributed deviate, with zero mean and unit variance [29], taken to be 5% of the maximum level of measured data. The cross sections of the three-dimensional model vector fields, phase curves, and the result of fields reconstruction on a plane $Y = 0$ are shown in Fig. 2 for the first model, in Fig. 3 for the second model. Phase curves in the secant plane are calculated using

$$\phi(x, z) = \arctan\left(\frac{g_z(x, z)}{g_x(x, z)}\right) \tag{22}$$

over three different paths: $z_1 = -0.49$, curve $(- + -)$, $z_2 = 0.02$, curve $(- \times -)$, $z_3 = 0.36$, curve $(- * -)$.

[2] $\lim_{x\to 0} = \frac{P_n^m(x)}{x} = 2^{m+1}\pi^{-1/2}\sin\left(\frac{\pi(m+n)}{2}\right)\frac{\Gamma\left(\frac{n+m}{2}+1\right)}{\Gamma\left(\frac{n-m}{2}+1/2\right)}$.

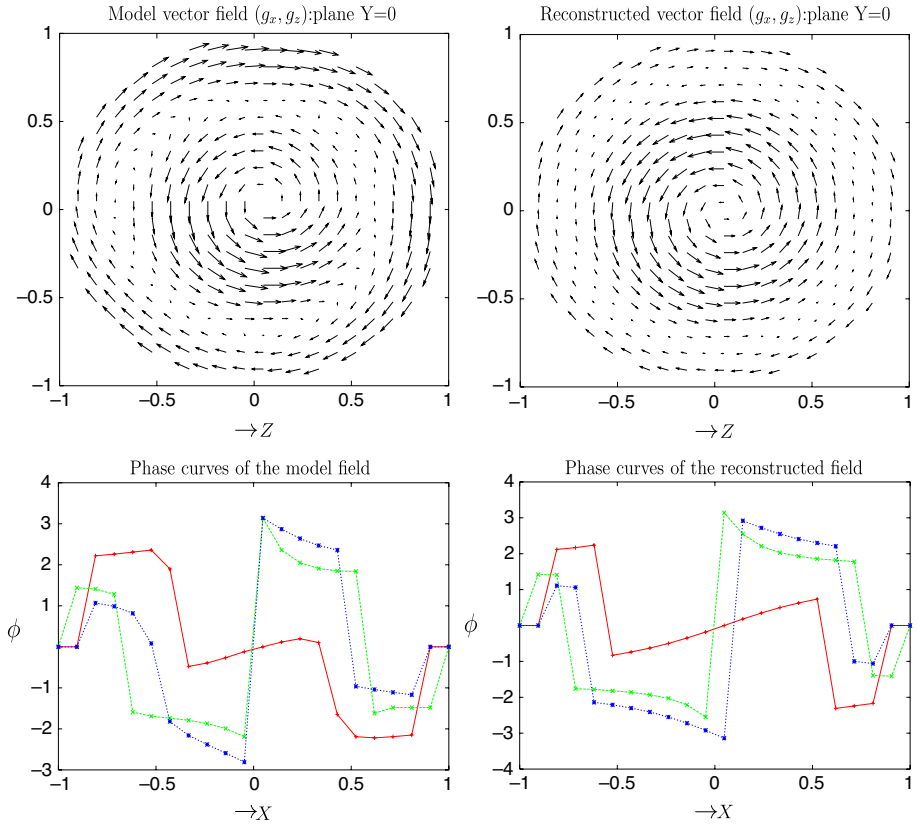

Fig. 2. The first model is defined by Eq. (20). Plane $x - z$: field (g_x, g_z) and corresponding phase curves for $z_1 = -0.49$, curve $(- + -)$, $z_2 = 0.02$, curve $(- \times -)$, $z_3 = 0.36$, curve $(- * -)$; exact (left) and reconstructed (right), fields.

A relative error of vector field reconstruction was calculated via

$$\epsilon = \frac{\sum\limits_{i,j,k} (\|\mathbf{g}(x_i, y_j, z_k)\| - \|\tilde{\mathbf{g}}(x_i, y_j, z_k)\|)^2}{\sum\limits_{i,j,k} \|\mathbf{g}(x_i, y_j, z_k)\|^2}, \tag{23}$$

where $i = 1 \div N_x$, $j = 1 \div N_y$, $k = 1 \div N_z$, $\|\cdot\|$ is a Euclidean norm.

Errors ϵ for 3D vector fields are 23% and 28% for the first and second models, respectively.

5. Conclusion

The paper has investigated the problem of reconstructing the 3D vector fields from linearly integrated data (vectorial ray-transform). Throughout the paper, vector spherical harmonics is used as basis vector-functions for vector field representation. This approach is quite convenient for our problem for several reasons. The first one is that VSHs forms orthonormal basis for solenoidal vector fields because of their properties (see Appendix B). The second feature is that the algorithm based on the VSHs decomposition regularizes computational process by cutting higher harmonic mode very easily. Finally our method take into account the spherical symmetry of the device and permit to plan experiment with sufficiently arbitrary geometry of the measurements. For spectral measurements, which often take place in spherical tokamak experiments, the problem is reduced to the Volterra integral equation of the first kind. Spectroscopic experimental data allows reconstruct only solenoidal component of a vector field, however, the irrotational component may be retrieved from the solution based on the boundary-value problem for the Laplace equation. Numerical computations on two different models have shown that the topology of the vector field is recovered with acceptable accuracy. The technique developed is means to be used for plasma flow velocity reconstruction in a spherical tokamak devices. There is strong interest in measuring the 3D plasma flow vectors in the whole volume of plasma experiments and the proposed method presents a solution for the solenoidal components.

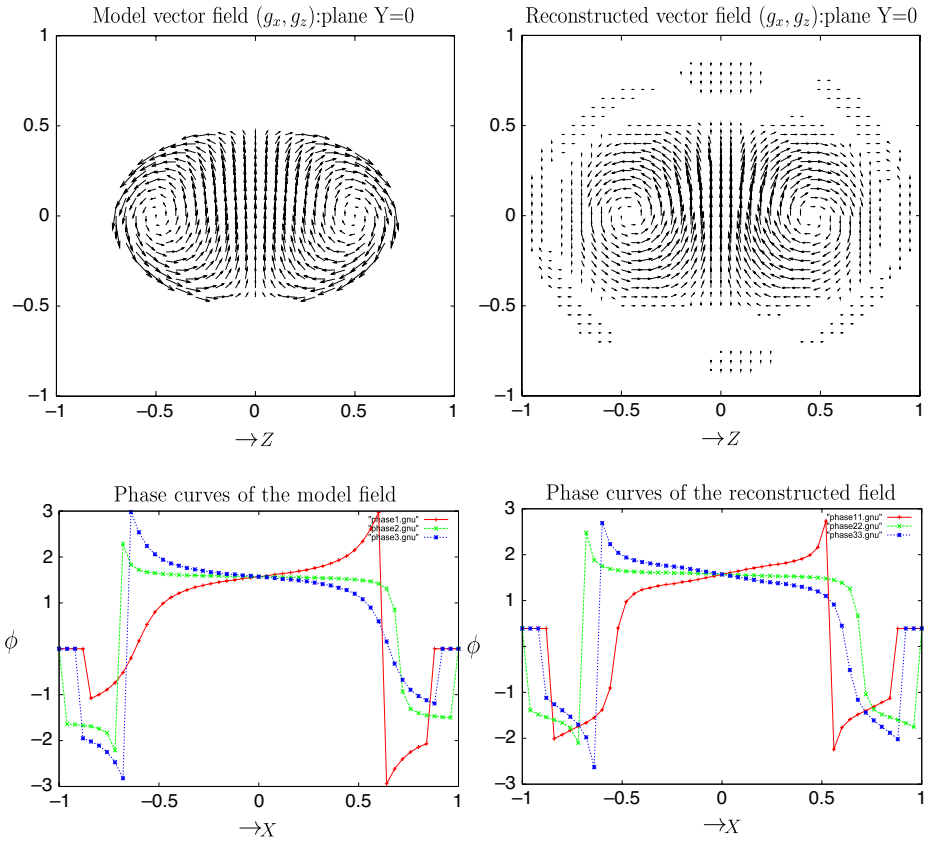

Fig. 3. The second model is derived from the analytical solution of the Grad–Shafranov equation and is described by Eqs. (21). Plane $x - z$: field (g_x, g_z) and corresponding phase curves for $z_1 = -0.49$, curve $(-+-)$, $z_2 = 0.02$, curve $(-\times-)$, $z_3 = 0.36$, curve $(-*-)$; exact (left) and reconstructed (right) fields.

Appendix A. Wigner *D*-functions

Matrices $D^J_{M_1 M_2}(\alpha, \beta, \gamma)$ are representations of the rotation group SO(3) and are normally expressed via a product of three functions, each depending only on one Euler angle (α, β, γ), i.e.,

$$D^J_{M_1 M_2}(\alpha, \beta, \gamma) = e^{-iM_1\alpha}\, d^J_{M_1 M_2}(\beta)\, e^{-iM_2\gamma}.$$

Here, $\alpha(0 \le \alpha < 2\pi)$ is the angle of rotation with respect to initial axis initial axis z, $\beta(0 \le \beta \le \pi)$ is the angle of rotation with respect to the new (rotated) axis y', and $\gamma(0 \le \gamma < 2\pi)$ is the angle of rotation with respect to the new (rotated) axis z'. All types of rotation of the coordinate system can be realized by consecutive rotations with respect to the axes z, y', and z', respectively, by the angles (α, β, γ). The real functions $d^J_{M_1 M_2}(\beta)$ have the following exact representation:

$$d^J_{M_1 M_2}(\beta) = (-1)^{M_1 - M_2}[(J + M_1)!(J - M_1)!(J + M_2)!(J - M_2)!]^{1/2} \times \sum_k (-1)^k \frac{(\cos\beta/2)^{2J-2k-M_1+M_2}(\sin\beta/2)^{2k+M_1-M_2}}{k!(J - M_1 - k)!(J + M_2 - k)!(M_1 - M_2 + k)!}.$$

The index k runs over all integer values for which the argument of the factorial has positive values, i.e.,

$$\max(0, M_2 - M_1) \le k \le \min(J - M_1, J + M_2)$$

(cf. [18]). Useful recurrent formulas for computing $d^J_{M_1}$ can be found in [20]. Edmonds in [17] came up with a method for calculating $D^J_{M_1 M_2}(\alpha, \beta, \gamma)$ for arbitrary values of arguments using the following relation:

$$D^J_{M_1 M_2}(\alpha, \beta, \gamma) = \sum_m e^{-iM_1\alpha} \cdot d^J_{M_1 m}(\pi/2) \cdot e^{-im\beta} \cdot d^J_{m M_2}(\pi/2) \cdot e^{-iM_2\gamma},$$

here, the values $d^J_{M_1 M_2}(\pi/2)$ can be calculated readily.

Appendix B. Vector spherical harmonics (VSHs): definition and some properties

The set of vectors $\mathbf{Y}_{JM}^{(\lambda)}$ with all positive integer values of $J (0 < J < \infty)$, $\lambda = -1, 0, 1$, and integer values of M, $|M| \leq J$, form a complete orthonormalized system in the space $\mathbf{L}_2(\mathbb{S}^2)$, $\mathbb{S}^2 := \{(\theta, \varphi | 0 \leq \theta < \pi, 0 \leq \varphi < 2\pi)\}$. In the paper, use is made of the VSHs defined in [18]: namely

$$\mathbf{Y}_{JM}^{(+1)}(\theta, \varphi) = \frac{1}{\sqrt{J(J+1)}} \nabla_{\Omega} Y_{JM}(\theta, \varphi) \tag{24}$$

$$\mathbf{Y}_{JM}^{(0)}(\theta, \varphi) = \frac{-i}{\sqrt{J(J+1)}} (\mathbf{e}_r \times \nabla_{\Omega}) Y_{JM}(\theta, \varphi), \tag{25}$$

$$\mathbf{Y}_{JM}^{(-1)}(\theta, \varphi) = \mathbf{e}_r Y_{JM}(\theta, \varphi), \tag{26}$$

$$\text{where } \nabla_{\Omega} = \frac{\partial}{\partial \theta} \mathbf{e}_{\theta} + \frac{1}{\sin\theta} \frac{\partial}{\partial \varphi} \mathbf{e}_{\varphi}.$$

Now, $\mathbf{Y}_{JM}^{(+1)}$ and $\mathbf{Y}_{JM}^{(0)}$ are transverse vectors with respect to the unit vector $\mathbf{e}_r = \mathbf{r}/r$, and $\mathbf{Y}_{JM}^{(-1)}$ is a longitudinal vector. We write

$$\mathbf{e}_r \cdot \mathbf{Y}_{JM}^{(+1)} = \mathbf{e}_r \cdot \mathbf{Y}_{JM}^{(0)} = 0, \qquad \mathbf{e}_r \times \mathbf{Y}_{JM}^{(-1)} = 0. \tag{27}$$

Normalization constants for VSHs with respect to the norm $\mathbf{L}^2(\Omega)$ are

$$\|\mathbf{Y}_{JM}^{(+1)}\|_{\mathbf{L}_2} = \|\mathbf{Y}_{JM}^{(0)}\|_{\mathbf{L}_2} = \|\mathbf{Y}_{JM}^{(-1)}\|_{\mathbf{L}_2} = \sqrt{\frac{4\pi}{(2J+1)} \frac{(J+M)!}{(J-M)!}} \tag{28}$$

An expansion of the vector functions $\mathbf{Y}_{JM}^{(\lambda)}(\theta, \varphi)$ with respect to the basis vectors $\mathbf{e}_r$, $\mathbf{e}_{\theta}$, and $\mathbf{e}_{\varphi}$ has the form

$$\mathbf{Y}_{JM}^{(\lambda)}(\theta, \varphi) = [\mathbf{Y}_{JM}^{(\lambda)}(\theta, \varphi)]_r \, \mathbf{e}_r + [\mathbf{Y}_{JM}^{(\lambda)}(\theta, \varphi)]_{\theta} \, \mathbf{e}_{\theta} + [\mathbf{Y}_{JM}^{(\lambda)}(\theta, \varphi)]_{\varphi} \, \mathbf{e}_{\varphi}. \tag{29}$$

Spherical components of the vectors $\mathbf{Y}_{JM}^{(\lambda)}(\theta, \varphi)$ are represented as follows [18]:

$$[\mathbf{Y}_{JM}^{(1)}(\theta, \varphi)]_r = 0, \tag{30}$$

$$[\mathbf{Y}_{JM}^{(1)}(\theta, \varphi)]_{\theta} = \frac{1}{\sqrt{J(J+1)}} \frac{\partial}{\partial \theta} Y_{JM}(\theta, \varphi),$$

$$[\mathbf{Y}_{JM}^{(1)}(\theta, \varphi)]_{\varphi} = \frac{1}{\sqrt{J(J+1)}} \frac{1}{\sin\theta} \frac{\partial}{\partial \varphi} Y_{JM}(\theta, \varphi) = \frac{iM}{\sqrt{J(J+1)}} \frac{1}{\sin\theta} Y_{JM}(\theta, \varphi),$$

$$[\mathbf{Y}_{JM}^{(0)}(\theta, \varphi)]_r = 0,$$

$$[\mathbf{Y}_{JM}^{(0)}(\theta, \varphi)]_{\theta} = \frac{i}{\sqrt{J(J+1)}} \frac{1}{\sin\theta} \frac{\partial}{\partial \varphi} Y_{JM}(\theta, \varphi) = \frac{-M}{\sqrt{J(J+1)}} \frac{1}{\sin\theta} Y_{JM}(\theta, \varphi),$$

$$[\mathbf{Y}_{JM}^{(0)}(\theta, \varphi)]_{\varphi} = -\frac{i}{\sqrt{J(J+1)}} \frac{\partial}{\partial \theta} Y_{JM}(\theta, \varphi).$$

$$[\mathbf{Y}_{JM}^{(-1)}(\theta, \varphi)]_r = Y_{JM}, \qquad [\mathbf{Y}_{JM}^{(-1)}(\theta, \varphi)]_{\theta} = 0, \qquad [\mathbf{Y}_{JM}^{(-1)}(\theta, \varphi)]_{\varphi} = 0.$$

The behavior of the vectors $\mathbf{Y}_{JM}^{(\lambda)}(\theta, \varphi)$ under rotation of the coordinate system is described by the equation

$$\mathbf{Y}_{JM_2}^{(\lambda)}(\boldsymbol{\omega}') = \sum_{|M_1| \leq J} D^J_{M_1 M_2}(\alpha, \beta, \gamma) \, \mathbf{Y}_{JM_1}^{(\lambda)}(\boldsymbol{\omega}). \tag{31}$$

Here $D^J_{M_1 M_2}(\alpha, \beta, \gamma)$ are Wigner D-functions (see Appendix A for definition and method of calculation); $\boldsymbol{\omega} = (\theta, \varphi)$ and $\boldsymbol{\omega}' = (\theta', \varphi')$ are unit vectors in, respectively, the initial (laboratory) and rotated (object-fitted) coordinate systems.

The orthogonality condition for $\mathbf{Y}_{JM}^{(\lambda)}(\theta, \varphi)$ is expressed as follows

$$\int_0^{\pi} \int_0^{2\pi} \mathbf{Y}_{J'M'}^{(\lambda')*}(\theta, \varphi) \mathbf{Y}_{JM}^{(\lambda)}(\theta, \varphi) \, \sin\theta \, d\theta d\varphi = \delta_{J'J} \delta_{\lambda'\lambda} \delta_{M'M}, \tag{32}$$

where the asterisk means complex conjugation and δ_{ij} is the Kronecker delta.

The following differential correspondences are used in the paper.

$$\begin{aligned}
&\nabla \times [f(r)\mathbf{Y}_{JM}^{(+1)}(\boldsymbol{\omega})] = i\left(\frac{d}{dr}+\frac{1}{r}\right) f(r)\mathbf{Y}_{JM}^{(0)}(\boldsymbol{\omega}),\\
&\nabla \cdot [f(r)\mathbf{Y}_{JM}^{(+1)}(\boldsymbol{\omega})] = -\sqrt{J(J+1)}\frac{f(r)}{r} Y_{JM}(\boldsymbol{\omega}),
\end{aligned} \tag{33}$$

$$\begin{aligned}
&\nabla \times [f(r)\mathbf{Y}_{JM}^{(0)}(\boldsymbol{\omega})] = i\left(\frac{d}{dr}+\frac{1}{r}\right) f(r)\mathbf{Y}_{JM}^{(+1)}(\boldsymbol{\omega}) + i\sqrt{J(J+1)}\frac{f(r)}{r}\mathbf{Y}_{JM}^{(-1)}(\boldsymbol{\omega}),\\
&\nabla \cdot [f(r)\mathbf{Y}_{JM}^{(0)}(\boldsymbol{\omega})] = 0,
\end{aligned} \tag{34}$$

$$\begin{aligned}
&\nabla \times [f(r)\mathbf{Y}_{JM}^{(-1)}(\boldsymbol{\omega})] = -i\sqrt{J(J+1)}\frac{f(r)}{r}\mathbf{Y}_{JM}^{(0)}(\boldsymbol{\omega}),\\
&\nabla \cdot [f(r)\mathbf{Y}_{JM}^{(-1)}(\boldsymbol{\omega})] = \left(\frac{d}{dr}+\frac{2}{r}\right) f(r) Y_{JM}(\boldsymbol{\omega}),
\end{aligned} \tag{35}$$

for any function $f(r)$ and $i = \sqrt{-1}$.

References

[1] J. Williamson, D. Evans, Computerized tomography for sparse-data plasma physics experiments, IEEE Trans. Plasma Sci. 10 (1982) 82.
[2] I.H. Hutchinson, Principle of Plasma Diagnostics, second ed., Cambridge University Press, Cambridge, 2005.
[3] Y. Nagayama, M. Yamada, W. Park, E.D. Fredrickson, A.C. Janos, K.M. McGuire, G. Taylor, Tomography of full sawtooth crashes on the tokamak fusion test reactor, Phys. Plasmas 3 (1996) 1647.
[4] F. Bonomo, P. Franz, G. Spizzo, L. Marelli, P. Martin, F. Paganucci, P. Rossetti, M. Signori, M. Andrenucci, N. Pomaro, Ultraviolet tomography of kink dynamics in a magnetoplasmadynamics truster, Phys. Plasmas 12 (2005) 3301.
[5] A.L. Balandin, V. Pickalov, G. Fuchs, Some applications of tomographic methods for vector fields, in: Proc. Int. Symp. on Computerized Tomography for Industrial Applications, Berlin, 1994.
[6] J. Howard, Vector tomography applications in plasma diagnostics, Plasma Phys. Control. Fusion 38 (1996) 489–503.
[7] A.L. Balandin, Y. Ono, Tomographic determination of plasma velocity with the use of ion Doppler spectroscopy, Eur. Phys. J. D 17 (2001) 337–344.
[8] A.L. Balandin, Y. Ono, Radial velocity profile reconstruction by Doppler spectroscopy measurements, Eur. Phys. J. D 27 (2003) 125–130.
[9] A.L. Balandin, Y. Ono, The method of series expansion for 3-D vector tomography reconstruction, J. Comput. Phys. 202 (2005) 52–64.
[10] W.W. Hansen, A new type of expansion in radiation problems, Phys. Rev. 47 (1935) 139–143.
[11] E.H. Hill, The theory of vector spherical harmonics, Amer. J. Phys. 22 (1954) 211–214.
[12] J. Blatt, V. Weisskopf, Theoretical Nuclear Physics, J. Wiley and Sons, 1952, p. 796. Appendix B.
[13] M.N. Jones, Atmospheric oscillations–I, Planet. Space Sci. 18 (1970) 1393–1416.
[14] M.N. Jones, Atmospheric oscillations–II, Planet. Space Sci. 19 (1971) 609–634.
[15] W. Freeden, T. Gervens, M. Schreiner, Constructive Approximation on the Sphere (With Applications to Geomathematics), Oxford Science Publication, Clarendon Press, 1998.
[16] J.D. Jackson, Classical Electrodynamics, J. Wiley and Sons, 1975.
[17] A.R. Edmonds, Angular Momentum in Quantum Mechanics, Princeton University Press, 1957.
[18] D.A. Varshalovich, A.N. Moskalev, V.K. Khersonskii, Quantum Theory of Angular Momentum, World Scientific Publishing, 1988.
[19] I.M. Gel'fand, Z.Y. Shapiro, Representation of the group of rotation in three-dimensional space and their applications, Amer. Math. Soc. Transl. 2 (1956) 207–316.
[20] L.C. Biedenharn, J.D. Louck, Angular Momentum in Quantum Physics. Theory and Applications, in: Encyclopedia of Mathematics and its Applications, vol. 8, Addison-Wesley Publishing, 1981.
[21] E.Yu. Derevtsov, S.G. Kazantsev, Th. Schuster, Polynomial bases for subspaces of vector fields in the unit ball. Method of ridge functions, J. Ill-Posed Probl. 15 (2007) 19–55.
[22] Jason Cantarella, Dennis DeTurck, Herman Gluck, Vector calculus and the topology of domains in 3-space, Amer. Math. Monthly 109 (5) (2002) 409–442.
[23] P. Temam, Navier–Stokes Equations, Theory and Numerical Analysis, Noth-Holland Publ., 1979.
[24] V.A. Sharafutdinov, Integral Geometry of Tensor Fields, VSP, Utrecht, 1994.
[25] Åke Björck, Numerical Methods for Least Squares Problems, SIAM, Philadelphia, 1996.
[26] A.D. Polyanin, A.V. Manzhirov, Handbook of Integral Equations, Chapman & Hall/CRC Press, 2008.
[27] Ling Wang, The X-ray transform and its inversion for the series expansion basis functions in three-dimensional tomography, SIAM J. Appl. Math. 52 (5) (1992) 1490–1499.
[28] P.M. Bellan, Fundamentals of Plasma Physics, Cambridge Univ. Press, 2006.
[29] W.H. Press, S.A. Teukolsky, W.T. Vetterling, B.P. Flannery, Numerical Recipes in FORTRAN, Cambridge Univ. Press, 1994.